

Electronic and vibrational properties of low-dimensional perovskites  $\text{Sr}_{1-y}\text{La}_y\text{NbO}_{3.5-x}$ 

C. A. Kuntzsch

Forschungszentrum Karlsruhe, Institut für Festkörperphysik, D-76021 Karlsruhe, Germany  
and 1. Physikalisches Institut, Universität Stuttgart, Pfaffenwaldring 57, D-70550 Stuttgart, Germany

S. Schuppler

Forschungszentrum Karlsruhe, Institut für Festkörperphysik, D-76021 Karlsruhe, Germany

P. Haas, B. Gorshunov, and M. Dressel

1. Physikalisches Institut, Universität Stuttgart, Pfaffenwaldring 57, D-70550 Stuttgart, Germany

M. G rioni

Institut de Physique Appliquée, École Polytechnique Fédérale, CH-1015 Lausanne, Switzerland

F. Lichtenberg

Experimentalphysik VI, Institut für Physik, EKM, Universität Augsburg, Universitätsstr. 1, D-86135 Augsburg, Germany  
(March 22, 2022)

By angle-resolved photoemission spectroscopy and polarization-dependent infrared reflectivity measurements the electronic and vibrational properties of low-dimensional perovskites  $\text{Sr}_{1-y}\text{La}_y\text{NbO}_{3.5-x}$  were studied along different crystal directions. The electronic behavior strongly depends on the oxygen and La content, including quasi-one-dimensional metallic and ferroelectric insulating behavior. An extremely small energy gap at the Fermi level is found for  $\text{SrNbO}_{3.41}$  and  $\text{SrNbO}_{3.45}$  along the conducting direction at low temperature, suggestive for a Peierls-type instability. Despite the similar nominal carrier density, for  $\text{Sr}_{0.8}\text{La}_{0.2}\text{NbO}_{3.50}$  the quasi-one-dimensional metallic character is suppressed and no gap opening is observed, which can be explained by differences in the crystal structure. Electron-phonon interaction appears to play an important role in this series of compounds.

## I. INTRODUCTION

The observation of quasi-one-dimensional (quasi-1D) metallic behavior of some members of the perovskite-related series  $\text{Sr}_{1-y}\text{La}_y\text{NbO}_{3.5-x}$ , with  $0 < x < 0.1$ , raised interest recently.<sup>1,2</sup> It comprises compounds with a wide range of electronic properties,<sup>3</sup> including a ferroelectric insulator, semiconducting compounds, and quasi-1D metals. They have an orthorhombic, perovskite-related crystal structure with lattice parameters  $a = 3.9$  Å,  $b = 5.5$  Å, and  $c$  depending on the oxygen content,<sup>3,5</sup> and belong to the homologous series of the type  $\text{Sr}_n\text{Nb}_n\text{O}_{3n+2}$ . The main building blocks of the structure are  $\text{NbO}_6$  octahedra, which are grouped into slabs extending along the  $(a,b)$  plane. The width of the slabs along  $c$  is determined by the oxygen content and directly given by the parameter  $n$ : While for quasi-1D metallic  $\text{SrNbO}_{3.40}$  ( $n=5$ ) the slabs are five octahedra wide, ferroelectric, insulating  $\text{SrNbO}_{3.50}$  ( $n=4$ ) consists of four octahedra wide slabs. For defined oxygen stoichiometries in the range  $0 < x < 0.1$  the structure exhibits a well-ordered stacking sequence of the  $(n=5)$ - and  $(n=4)$ -subunits, listed in Table I for the investigated compounds.<sup>3,5,6</sup> A schematic drawing of the idealized crystal structure of three representative  $\text{SrNbO}_{3.50-x}$  compounds is shown in Fig. 1. The real crystal structure exhibits a considerable distortion of the  $\text{NbO}_6$  octahedra, with different magnitude

TABLE I. Studied niobates of the type  $\text{Sr}_n\text{Nb}_n\text{O}_{3n+2}$ . For each composition the stacking sequence of the  $(n=5)$ - and  $(n=4)$ -subunits per unit cell and the nominal number  $z$  of Nb4d conduction electrons per formula unit are given.

	stacking sequence	$z$
$\text{SrNbO}_{3.41}$	-5-5-5-5-	0.18
$\text{SrNbO}_{3.45}$	-4-5-4-5-	0.1
$\text{SrNbO}_{3.50}$	-4-4-4-4-	0
$\text{Sr}_{0.8}\text{La}_{0.2}\text{NbO}_{3.50}$	-4-4-4-4-	0.2
$\text{Sr}_{0.7}\text{Ba}_{0.1}\text{La}_{0.2}\text{NbO}_{3.50}$	-4-4-4-4-	0.2
$\text{Sr}_{0.6}\text{Ca}_{0.2}\text{La}_{0.2}\text{NbO}_{3.50}$	-4-4-4-4-	0.2

depending on the position within the slab. Along the  $a$  axis the octahedra are connected continuously via the apical oxygen sites forming 1D chains, as is illustrated in Ref. 2. The oxygen content not only determines the crystal structure but also the number of Nb4d conduction electrons. A second doping channel which, however, does not affect the width and stacking sequence of the slabs is the substitution of divalent Sr by a higher-valent element like La. The nominal numbers of Nb4d conduction electrons per formula unit for the present niobates, derived within an ionic picture, are listed in Table I.

According to dc resistivity measurements, the electronic properties of  $\text{SrNbO}_{3.41}$  and  $\text{Sr}_{0.8}\text{La}_{0.2}\text{NbO}_{3.50}$  are

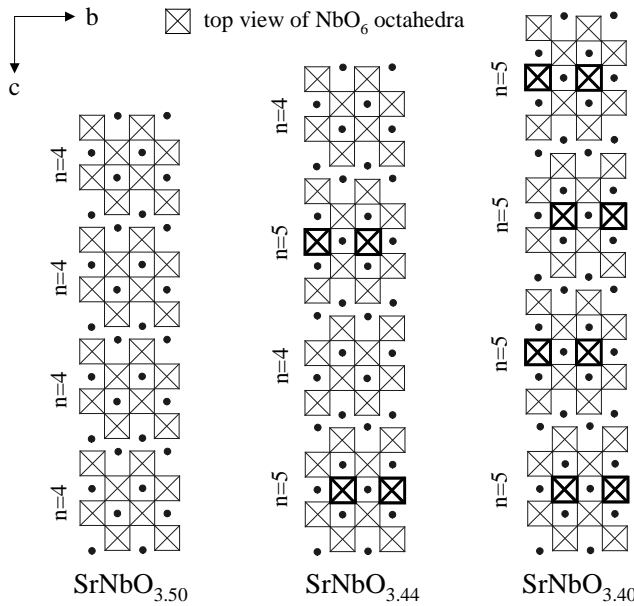


FIG. 1. Schematic drawing of the idealized, i.e., non-distorted, crystal structures of three compounds of the series  $\text{Sr}_n\text{Nb}_n\text{O}_{3n+2}$ . The  $\text{NbO}_6$  units in the middle of the slabs, which presumably are the conducting channels of the lattice, are marked by thick lines.

highly anisotropic, with lowest, metal-like resistivity values along the  $a$  direction.<sup>3</sup> The temperature dependence of the resistivity along the  $a$  axis,  $\rho_a$ , consists of several regimes; taking  $\text{SrNbO}_{3.41}$  as an example, one observes the following behavior: Starting from the lowest temperature, the resistivity decreases strongly, showing a minimum around 50 K and increases between 50 and 130 K. Above 130 K  $\rho_a$  decreases slightly with increasing temperature. The resistivity behavior below 50 K can be described by an activated behavior  $\rho \propto \exp[E_a/(k_B T)]$  with activation energies  $E_a = 2\text{--}3\text{ meV}$ .<sup>2,3</sup> An explanation for the temperature behavior of  $\rho_a$  above 50 K is so far missing. A similar temperature dependence is observed for  $\text{Sr}_{0.8}\text{La}_{0.2}\text{NbO}_{3.50}$ .

On the other hand,  $\text{SrNbO}_{3.50}$  ( $n=4$ ) is a band insulator. It is ferroelectric below  $T_c = 1613\text{ K}$  with a spontaneous polarization along the  $b$  axis.<sup>7,8</sup> The compound undergoes two further phase transitions, namely a second-order phase transition to an incommensurate phase at 488 K and another ferroelectric transition at 117 K with an additional component of the spontaneous polarization appearing along the  $c$  axis.<sup>9</sup>

The magnetic properties of the investigated niobium oxide compounds were described in Ref. 3. Except  $\text{SrNbO}_{3.50}$ , all compounds show a similar behavior: With increasing temperature, between 4 and 50 K the magnetic susceptibility decreases steeply due to paramagnetic impurities, followed by an increase between 50 and 400 K. This increase is not yet understood; explanations in terms of thermally activated charge carriers excited across an energy gap or the Bonner-Fisher model for

a 1D antiferromagnetic spin-1/2 Heisenberg spin chain were proposed.<sup>10</sup>

The conduction mechanism of the compounds  $\text{SrNbO}_{3.41}$ ,  $\text{SrNbO}_{3.45}$ , and  $\text{Sr}_{0.8}\text{La}_{0.2}\text{NbO}_{3.50}$  was studied by dielectric measurements in the radio-frequency range along the  $c$  direction.<sup>11</sup> They suggest a hopping transport of charge carriers with polaronic character along  $c$ . The results from EPR studies on  $\text{SrNbO}_{3.41}$ <sup>10</sup> with the magnetic field applied parallel to the  $b$  and  $c$  axis are in agreement with a variable range hopping in 1D. Furthermore,  $^{93}\text{Nb}$  NMR measurements indicate a fluctuating quadrupole field and seem to resemble some of the characteristics of the prototypical charge-density-wave (CDW) compound  $\text{NbSe}_3$ .<sup>10</sup>

The most puzzling finding for the series  $\text{Sr}_{1-y}\text{La}_y\text{NbO}_{3.50-x}$  is an extremely small energy gap at the Fermi energy for  $\text{SrNbO}_{3.41}$  along the chain direction.<sup>2</sup> In this manuscript we will show that signatures of a very small energy gap are also present for the compound  $\text{SrNbO}_{3.45}$ . In order to understand the observed quasi-1D metallic character and the unusual properties at low temperature, we give an overview of the electronic and vibrational properties of various compounds of the series  $\text{Sr}_{1-y}\text{La}_y\text{NbO}_{3.50-x}$ , as obtained by optical spectroscopy in the infrared frequency range and angle-resolved photoemission spectroscopy (ARPES). We will discuss our findings for the various compounds with respect to differences in the crystal structure. Based on the comparison of our results from optics and ARPES to the dc resistivity data, we propose a possible picture for the transport mechanism and discuss the role of electron-phonon coupling in these niobate compounds.

The manuscript is organized as follows: The experimental details are given in Sec. II, followed by the presentation of the experimental results in Sec. III. We discuss the electronic and vibrational properties of the series  $\text{Sr}_{1-y}\text{La}_y\text{NbO}_{3.50-x}$  in Sec. IV and conclude with a summary of the findings in Sec. V.

## II. EXPERIMENT

The investigated  $\text{SrNbO}_{3.41}$ ,  $\text{SrNbO}_{3.45}$ ,  $\text{SrNbO}_{3.50}$ , and  $(\text{Sr,Ba,Ca})_{0.8}\text{La}_{0.2}\text{NbO}_{3.50}$  single crystals with a typical size of  $3 \times 2 \times 0.2\text{ mm}^3$  were grown by a coating zone melting process, and their oxygen content was determined by thermogravimetric analysis.<sup>3</sup> ARPES data were recorded with a Scienta ESCA-300 analyzer. The He I (21.22 eV) line of a standard gas discharge lamp was used. With a fixed analyzer setup the sample was rotated around one axis; the rotation angle determines the emission direction of the photoelectrons relative to the surface normal and thus the component  $k$  of the photoelectron momentum along the studied direction according to  $k = \frac{2m E_{kin}}{\hbar} \sin \theta = h$ . The crystals, which had been oriented to  $\{111\}$  by Laue diffraction before introducing them into the UHV system, were cleaved at a base pres-

sure of  $1 \cdot 10^{-10}$  mbar and cooled down. ARPES spectra with energy resolution  $E = 30$  meV were recorded at temperature  $T = 75$  K. The sample surface quality was checked periodically by comparison of valence band features. The angular resolution of the ARPES spectra amounts to  $\Delta\theta = 0.5^\circ$  corresponding to  $k = 0.04 \text{ \AA}^{-1}$ . The Fermi energy  $E_F$  was determined to 1 meV accuracy from the Fermi cut-off of a freshly evaporated gold film recorded immediately afterwards at the same experimental conditions.

For the reactivity measurements the samples were carefully polished on a polishing disc using diamond paste with a grain size of 1  $\mu\text{m}$  to obtain flat and shiny surfaces. Near-normal incidence reflection measurements with the electric field  $E$  of the incident light parallel to the  $a$  and  $b$  axes were performed for frequencies 20–10 000  $\text{cm}^{-1}$  using a Fourier-transform spectrometer Bruker IFS 113v. The energy resolution was set to 1  $\text{cm}^{-1}$  in the far-infrared range and to 2–4  $\text{cm}^{-1}$  in the mid-infrared (MIR) and near-infrared range. For  $\text{SrNbO}_{3.41}$ ,  $\text{SrNbO}_{3.45}$ , and  $\text{Sr}_{0.8}\text{La}_{0.2}\text{NbO}_{3.50}$  the low frequency reactivity (6–30  $\text{cm}^{-1}$ ) was studied with a quasi-optical submillimeter (submm) spectrometer<sup>12</sup> using backward-wave oscillators which produce monochromatic, polarized radiation continuously tunable in frequency. For  $\text{SrNbO}_{3.41}$  the reactivity spectra were extended to 34 000  $\text{cm}^{-1}$  by utilizing a Bruker IFS 66v/S spectrometer. The use of optical cryostates enabled temperature-dependent measurements between 5 and 300 K. To obtain absolute reactivities the spectra were divided by the reactivity spectra of an Al mirror.

To obtain the optical conductivity  $\sigma_1(\omega)$  by Kramers-Kronig analysis the reactivity spectra  $R(\omega)$  of  $\text{SrNbO}_{3.41}$  and  $\text{SrNbO}_{3.45}$  along the highly conducting direction were extrapolated to zero frequency according to the Hagen-Rubens relation.<sup>13</sup> A constant extrapolation to  $\omega = 0$  was chosen for the perpendicular direction. For insulating  $\text{SrNbO}_{3.50}$  the value  $R(0)$  for the constant low-frequency extrapolation was calculated from the dielectric constant  $\epsilon_1$  at 1 kHz ( $\epsilon_{1,a} = 75$ ,  $\epsilon_{1,b} = 43$ )<sup>8</sup> according to  $R(0) = [(1 - \frac{1}{\epsilon_1}) / (1 + \frac{1}{\epsilon_1})]^2$ . For the  $\text{Sr}_{0.2}\text{La}_{0.8}\text{NbO}_{3.50}$  spectra either a Hagen-Rubens or a constant extrapolation was used, depending on the low-frequency behavior of the measured reactivity at different temperatures. For the high-frequency extrapolation of all spectra an  $\omega^{-4}$  decay was assumed.

In the case of  $\text{SrNbO}_{3.45}$  the reactivity data were supplemented by transmission measurements in the frequency range 10–20  $\text{cm}^{-1}$  on a single crystal of thickness 20  $\mu\text{m}$  using a Mach-Zehnder interferometer arrangement. From the independent determination of the transmission coefficient and the phase shift we were able to directly calculate the complex dielectric function  $\epsilon(\omega)$  by utilizing the Fresnel equations.<sup>12</sup>

In the case of  $\text{SrNbO}_{3.45}$  the reactivity data were supplemented by transmission measurements in the frequency range 10–20  $\text{cm}^{-1}$  on a single crystal of thickness 20  $\mu\text{m}$  using a Mach-Zehnder interferometer arrangement. From the independent determination of the transmission coefficient and the phase shift we were able to directly calculate the complex dielectric function  $\epsilon(\omega)$  by utilizing the Fresnel equations.<sup>12</sup>

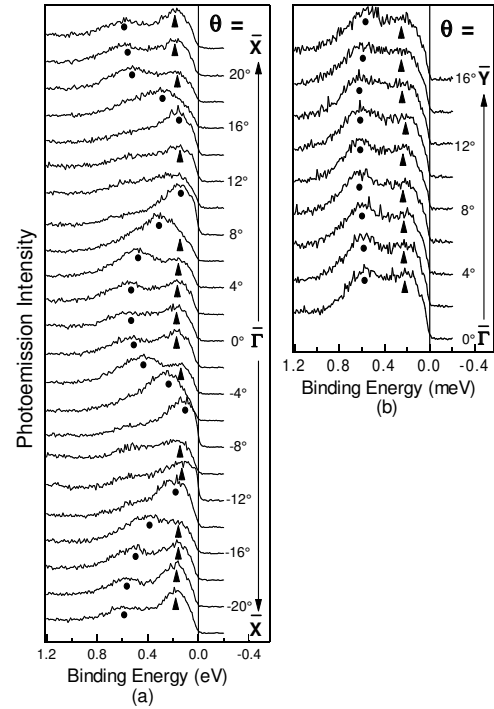


FIG. 2. ARPES spectra of  $\text{SrNbO}_{3.41}$ , normalized to the same total intensity, along (a)  $-X$  and (b)  $-Y$  at 75 K with  $E = 30$  meV.

### III. RESULTS

#### A. $\text{SrNbO}_{3.41}$ : ARPES, optics

The  $k$ -dependent near- $E_F$  electronic structure, as studied by ARPES, reflects the strongly anisotropic character of  $\text{SrNbO}_{3.41}$  (see Fig. 2): One observes two bands near  $E_F$ , with 600 and 200 meV binding energy (BE) at the  $\Gamma$  point. Along  $-X$  (Fig. 2a), i.e., along the chains, the band at lower BE shows no dispersion, whereas the second band disperses strongly towards  $E_F$ , gains intensity at around  $j \approx 8$ , and loses intensity between  $j \approx 8$  and  $j \approx 10$  suggestive of a Fermi surface (FS) crossing. At  $j \approx 14$  the peak reappears and disperses away from  $E_F$  for higher  $j$ . The reappearance of the peak can be explained in terms of a  $2 \times 1$  superstructure which was also observed by low energy electron diffraction<sup>1,14</sup> and neutron scattering,<sup>15</sup> and seems to be a characteristic property of all members of the  $\text{Sr}_{1-y}\text{La}_y\text{NbO}_{3.5-x}$  series. The parabolic dispersion of the band around  $\Gamma$  and  $X$  gives an effective electron mass of  $m/m_0 = 0.71$ . Along the perpendicular direction  $-Y$  (Fig. 2b) both bands hardly show any dispersion.

The anisotropic character is confirmed by the strongly polarization-dependent reactivity  $R(\omega)$  shown in Fig. 3. It exhibits a plasma edge for  $E_{ka}$  and high values  $R(\omega)$  at low frequencies indicating metallic behavior. In contrast, for  $E_{kb}$  the considerably lower reactivity demonstrates the insulating character perpendicular to the chains. The

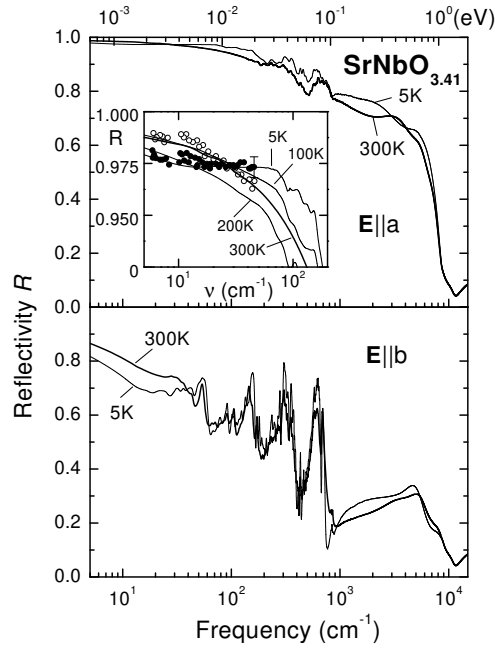


FIG. 3. Reflectivity  $R$  of  $\text{SrNbO}_{3.41}$  at different temperatures for  $E||a$  and  $E||b$ , respectively. Inset: Low-frequency reflectivity for  $E||a$ ; open (closed) circles: submm reflectivity data at 300 K (5 K).

corresponding optical conductivity  $\sigma_1$  (Fig. 4) for  $E||a$  consists of a Drude-like component followed by phonon modes and a relatively broad MIR band centered around  $1500 \text{ cm}^{-1}$ . A rich phonon spectrum is observed along both directions; for  $E||b$  76 lines can be resolved at RT, with the strongest modes at 144, 296, 304, 561, 572, 577, 583, 595, 603, 612, and  $680 \text{ cm}^{-1}$ . The strong double-peak structure in the  $E||b$  spectrum centered around  $5000 \text{ cm}^{-1}$  can be related to interband transitions.

During cooling down considerable changes can be seen in the electronic and vibrational part of the spectra: For  $E||b$  at least six new modes appear with decreasing temperature. Along the perpendicular direction,  $E||a$ , a strong peak appears around  $40 \text{ cm}^{-1}$  in the optical conductivity spectrum (see Fig. 4), which starts building up below 100 K. With decreasing temperature the peak shifts slightly to higher frequencies and becomes stronger. As discussed in Ref. 2 this feature can be ascribed to single-particle excitations across a gap in the electronic density of states (DOS) with  $2 \text{ (5 K) } 5 \text{ meV}$ . The development of the peak is already indicated in the reflectivity at 5 K by the lowering and flattening of the low-frequency part of the spectrum (see inset of Fig. 3). The gap opening at low temperature strongly influences the dielectric constant  $\epsilon_1(\omega \rightarrow 0)$ : Assuming a simple picture of a semiconductor with an energy gap  $\hbar\omega_g$  between the narrow valence and conduction band, the relation  $\epsilon_1(\omega \rightarrow 0) \propto \omega_g^2$  is expected to hold.<sup>13</sup> This explains the measured spectrum  $\epsilon_1(\omega)$  of  $\text{SrNbO}_{3.41}$  for  $E||a$  (Fig. 5), where at 5 K high positive values are found for  $\omega \rightarrow 0$ . In contrast, at 300 K  $\epsilon_1(\omega \rightarrow 0)$  is negative as expected for a metal.

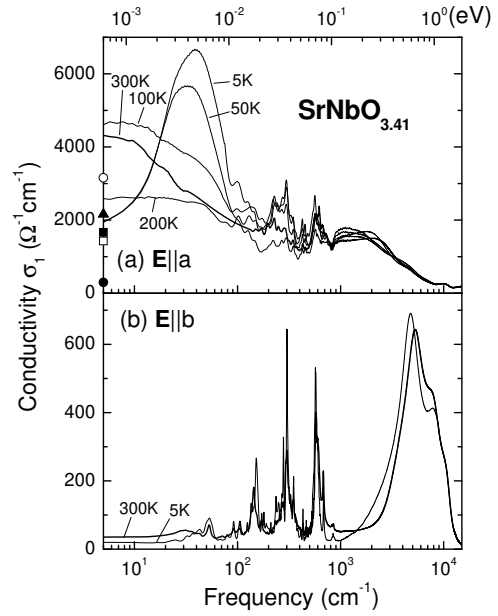


FIG. 4. Optical conductivity  $\sigma_1$  of  $\text{SrNbO}_{3.41}$  at different temperatures for  $E||a$  and  $E||b$ , respectively. For  $E||a$  the low-temperature peak around  $40 \text{ cm}^{-1}$  indicates excitations across a gap  $2 \text{ (5 meV)}$ . Also shown are the dc conductivity values for the  $a$  axis at 300 K (filled triangle), 200 K (open square), 100 K (filled square), 50 K (open circle), and 5 K (filled circle).

These findings confirm the high-resolution ARPES data, which show a gap between the leading edge midpoint of the spectrum and  $E_F$  of  $(25 \text{ K}) 4 \text{ meV}$  for  $X^2$ . The gap opening as observed by optics and ARPES along the chain direction is in agreement with the dc resistivity data along the  $a$  direction, although there the upturn occurs at a lower temperature ( $50 \text{ K}$ ) than the development of the low-frequency peak in the optical conductivity (below 100 K), as was already pointed out in Ref. 2. In Fig. 4 we also included the dc conductivity results;<sup>3</sup> above 50 K the dc values are obviously lower than the optical conductivity values at  $5 \text{ cm}^{-1}$ . This suggests that the optical conductivity  $\sigma_1$  cannot be described by a simple Drude-type behavior. Fitting the  $\sigma_1(\omega)$ -spectra with the Drude-Lorentz model indeed shows that a fit of reasonable quality (not shown) requires the introduction of two Drude peaks, e.g., with  $\gamma_{1,1}(\omega \rightarrow 0) = 2006 \text{ cm}^{-1}$  and  $\gamma_{1,2}(\omega \rightarrow 0) = 2356 \text{ cm}^{-1}$  at 300 K, which is in good agreement with the corresponding dc conductivity value.

#### B. $\text{SrNbO}_{3.50}$ : Optics

The reflectivity spectra of  $\text{SrNbO}_{3.50}$  (insets of Fig. 6) are significantly different from those of  $\text{SrNbO}_{3.41}$ . The overall low reflectivity for both polarization directions is in accordance with the insulating nature of the material. The non-conducting character is also illustrated in

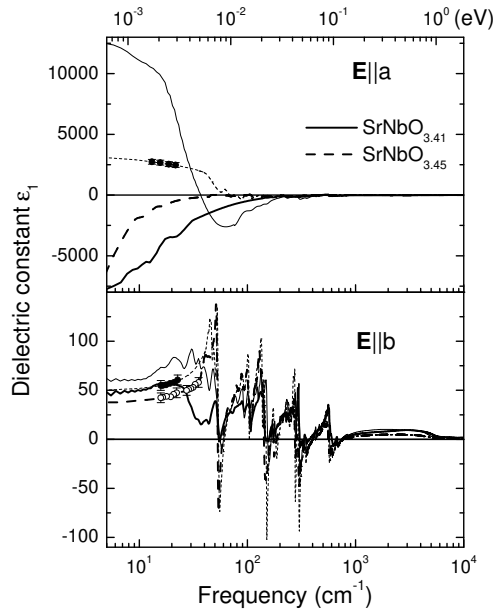


FIG. 5. Dielectric constant  $\epsilon_1$  of  $\text{SrNbO}_{3.41}$  and  $\text{SrNbO}_{3.45}$  at 300 K (thick lines) and 5 K (thin lines) for Eka and Ekb, respectively; open (closed) circles: data points at 300 K (5 K) directly determined by transmission measurements on a thin platelet.

the optical conductivity spectra (Fig. 6) which do not contain electronic excitations in the low-frequency range (the onset of interband transitions is around  $2000 \text{ cm}^{-1}$  for both polarizations) but only vibrational excitations. Perpendicular to the chains, i.e., for Ekb, a rich phonon spectrum is found. At RT one can resolve 24 infrared active modes for Ekb, with the strongest around 54, 100, 147, 176, 275, 295, 338, 567, and  $601 \text{ cm}^{-1}$ , and 12 modes for Eka, the strongest being around 112, 173, 295, and  $561 \text{ cm}^{-1}$ . A qualitative assignment of the phonon modes is given in the discussion. The mode around  $54 \text{ cm}^{-1}$  for Ekb is close to the soft mode found by Raman scattering experiments<sup>16</sup> which is related to the ferroelectric transition at 1615 K. It is expected to be infrared active, and indeed was already observed in earlier reactivity and transmission studies.<sup>17</sup> During cooling down additional modes appear in agreement with the results of Ref. 17, and at 5 K there are altogether 24 and 51 modes resolved for Eka and Ekb, respectively. The number of observed modes at RT and 5 K is lower than expected from the factor group analysis;<sup>17</sup> the missing modes might be either masked by the other contributions or too weak to be resolved.

### C. $\text{SrNbO}_{3.45}$ : Optics

Previous ARPES measurements<sup>1;18</sup> on  $\text{SrNbO}_{3.45}$  revealed a quasi-1D band structure near  $E_F$  similar to that of  $\text{SrNbO}_{3.41}$ . Also the optical response shown in Fig. 7 clearly demonstrates strong similarities in the electronic

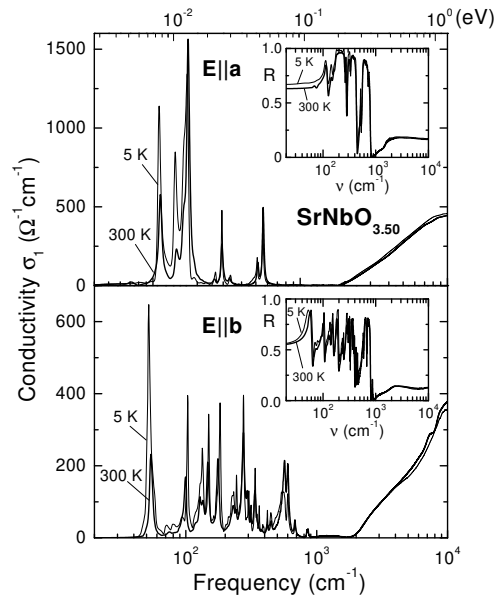


FIG. 6. Optical conductivity  $\sigma_1$  of  $\text{SrNbO}_{3.50}$  at 300 and 5 K for Eka and Ekb, respectively. Insets: Reactivity  $R$  used for Kramers-Kronig analysis.

properties between the two compounds: The Eka reactivity  $R$  at RT is high and almost 1 at low frequencies and shows a pseudo plasma edge, whereas for Ekb the overall reactivity is low and no plasma edge is found. Correspondingly, for Eka the optical conductivity contains a Drude-like peak due to itinerant electrons which is superimposed by vibrational modes between 50 and  $800 \text{ cm}^{-1}$ , followed by a pronounced MIR band centered around  $2000 \text{ cm}^{-1}$  with a vibrational fine structure. In contrast, for Ekb no Drude peak is observed in  $\sigma_1(\omega)$  but a large number of vibrational excitations up to  $900 \text{ cm}^{-1}$  followed by interband transitions above  $2000 \text{ cm}^{-1}$ . Thus, also  $\text{SrNbO}_{3.45}$  shows a quasi-1D metallic character at RT, with a metal-like behavior along the chains and an insulating behavior along the perpendicular direction.

The temperature dependence of the low-frequency optical properties along the chains agrees qualitatively with the dc resistivity,<sup>19</sup> being almost temperature-independent between 300 K and 100 K and increases below 100 K with decreasing temperature. Substantial changes occur in the low-frequency ( $< 50 \text{ cm}^{-1}$ ) optical response of  $\text{SrNbO}_{3.45}$  at low temperatures ( $< 100 \text{ K}$ ): One observes a lowering and attenuating of the reactivity (see inset of Fig. 7) which signals the development of a new excitation. According to the optical conductivity (Fig. 7) between 0 and  $400 \text{ cm}^{-1}$  a redistribution of spectral weight from low to high frequencies occurs for temperatures below 150 K, resulting in the development of a relatively broad and asymmetric peak, which has a maximum around  $60 \text{ cm}^{-1}$  ( $\sim 7 \text{ meV}$ ) and is superimposed by a large number of phonon excitations. The peak intensity increases with decreasing temperature. One can

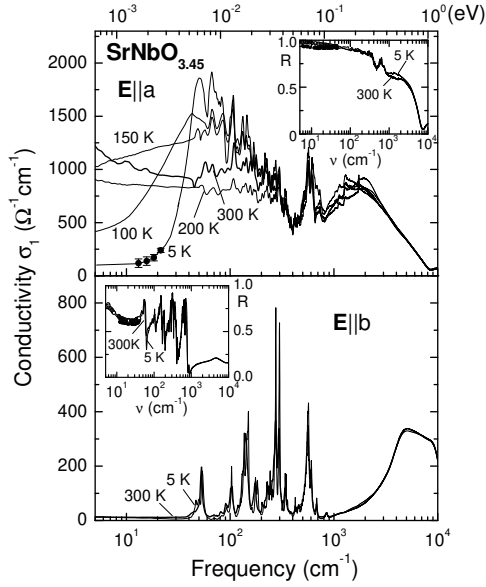


FIG. 7. Optical conductivity  $\sigma_1$  of  $\text{SrNbO}_{3.45}$  at different temperatures for E||a and E||b, respectively; closed circles: data points directly determined by transmission measurements on a thin platelet. For E||a the low-temperature peak in  $\sigma_1$  with its maximum around  $60 \text{ cm}^{-1}$  indicates excitations across a gap  $2-7 \text{ meV}$ . Insets: Real activity  $R$  used for Kramers-Kronig analysis; open (closed) circles: submm reactivity data at 300 K (5 K).

ascribe the development of the low-frequency peak to the opening of an energy gap with decreasing temperature. The presence of a small gap at low temperature is also indicated by the high values of the corresponding dielectric constant  $\epsilon_1$  at 5 K for  $\theta = 0$  (Fig. 5), as was discussed for  $\text{SrNbO}_{3.41}$  in section III A. In summary,  $\text{SrNbO}_{3.45}$  resembles the electronic properties of  $\text{SrNbO}_{3.41}$  by showing both a quasi-1D metallic character and the opening of an energy gap of only a few meV size below 150 K.

#### D. $\text{Sr}_{0.8}\text{La}_{0.2}\text{NbO}_{3.50}$ : ARPES, optics

The electronic properties of  $\text{Sr}_{0.8}\text{La}_{0.2}\text{NbO}_{3.50}$  near  $E_F$  were studied by ARPES along the two high-symmetry lines  $\bar{X}$  and  $\bar{Y}$ ; the results are depicted in Fig. 8. At the  $\Gamma$  point we observe a broad peak around 350 meV BE. Along  $\bar{X}$  the peak slowly disperses towards  $E_F$  accompanied by an intensity increase and between  $j = 7$  and  $j = 9$  the intensity of the peak slightly drops; at higher emission angles a broad peak is still visible with almost constant BE ( $\sim 350 \text{ meV}$ ). Along  $\bar{Y}$  no dispersion of the broad peak is observed. Along both directions and for all emission angles the overall photoelectron intensity near  $E_F$  is quite low. We also studied the ARPES spectra for  $\text{Sr}_{0.7}\text{La}_{0.2}\text{Ba}_{0.1}\text{NbO}_{3.50}$  and  $\text{Sr}_{0.6}\text{La}_{0.2}\text{Ca}_{0.2}\text{NbO}_{3.50}$  (not shown), having the same nominal carrier density as  $\text{Sr}_{0.8}\text{La}_{0.2}\text{NbO}_{3.50}$  (see Table I): For these two compounds the dispersion of the broad peak along  $\bar{X}$  for

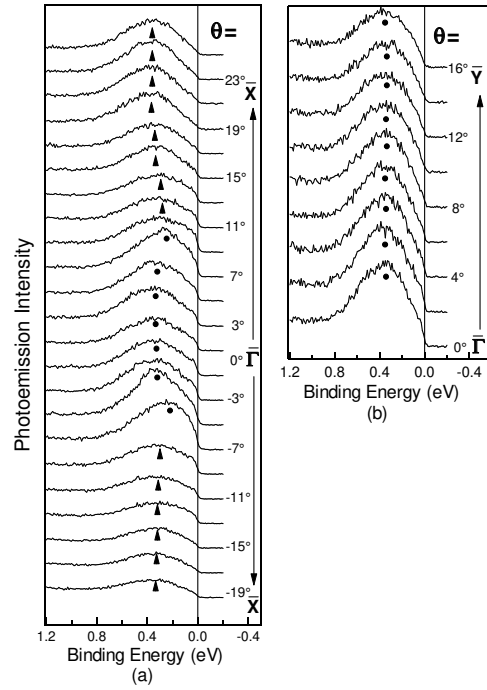


FIG. 8. ARPES spectra of  $\text{Sr}_{0.8}\text{La}_{0.2}\text{NbO}_{3.50}$  along (a)  $\bar{X}$  and (b)  $\bar{Y}$  at 75 K with  $E = 30 \text{ meV}$ .

$j = 7$  is even less pronounced.<sup>14</sup> The results for the  $(\text{Sr,Ba,Ca})_{0.8}\text{La}_{0.2}\text{NbO}_{3.50}$  suggest that there are two near- $E_F$  bands with similar BEs: One band is almost dispersionless along both  $\bar{X}$  and  $\bar{Y}$ ; the second band has a parabolic-like dispersion, although very weak, along  $\bar{X}$  with an intensity drop near  $E_F$  suggestive of a FS crossing, and is dispersionless along  $\bar{Y}$ . To some extent the band dispersions of  $\text{Sr}_{0.8}\text{La}_{0.2}\text{NbO}_{3.50}$  thus resemble those of  $\text{SrNbO}_{3.41}$  (see Fig. 2). However, compared to  $\text{SrNbO}_{3.41}$  the dispersion along  $\bar{X}$  is much weaker, i.e., the quasi-1D character of the band structure is less developed.

Further insight was gained by temperature-dependent reactivity measurements for E||a; b (see Fig. 9). For the polarization E||b the overall low reactivity and the absence of a Drude component in  $\epsilon_1(\omega)$  demonstrate the insulating character of the material perpendicular to the chains. For E||a the reactivity at RT is metal-like with relatively high values at low frequencies, decreases for higher frequencies, and finally drops rapidly above  $6000 \text{ cm}^{-1}$ . The corresponding optical conductivity shows a very weak Drude-like contribution and a pronounced MIR absorption peak around  $3000 \text{ cm}^{-1}$ . Between 300 K and 50 K the low-frequency optical conductivity is in reasonable agreement with the dc conductivity,<sup>3</sup> but at 5 K it is lower than the dc value. The overall optical response of  $\text{Sr}_{0.8}\text{La}_{0.2}\text{NbO}_{3.50}$  is similar to that of  $\text{SrNbO}_{3.41}$  (see Fig. 4) and  $\text{SrNbO}_{3.45}$  (see Fig. 7), but there are important differences: The overall reactivity of  $\text{Sr}_{0.8}\text{La}_{0.2}\text{NbO}_{3.50}$  along the chains is lower in the far-infrared range and the plasma edge is hardly devel-

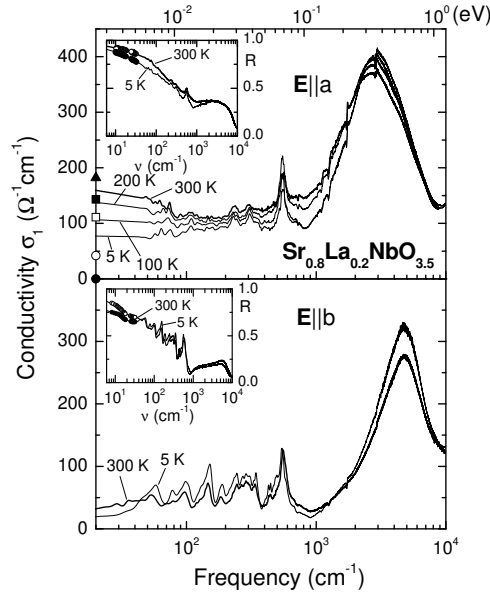


FIG. 9. Optical conductivity  $\sigma_1$  of  $\text{Sr}_{0.8}\text{La}_{0.2}\text{NbO}_{3.50}$  at different temperatures for Eka and Ekb, respectively. Also shown are the dc conductivity values for the a axis at 300 K (filled triangle), 200 K (open square), 100 K (filled square), 50 K (open circle), and 5 K (filled circle). Insets: Re c tivity R used for Kramers-Kronig analysis; open (closed) circles: submm re c tivity data at 300 K (5 K).

oped; both findings indicate only weak metallic character. Thus, the optical conductivity of  $\text{Sr}_{0.8}\text{La}_{0.2}\text{NbO}_{3.50}$  for Eka contains a much weaker Drude-like term. Importantly, with decreasing temperature the development of a low-frequency peak is not observed, in contrast to what is found for  $\text{SrNbO}_{3.41}$  and  $\text{SrNbO}_{3.45}$  (see Figs. 4 and 7).

#### IV. DISCUSSION

According to the experimental results, the electronic properties of the  $\text{SrNbO}_{3.50}$  compounds strongly depend on the oxygen content, which not only determines the crystal structure, but also the number of conduction electrons in the material (see Table I). To illustrate these differences we plot in Fig. 10 the optical conductivity at RT for the three compositions  $\text{SrNbO}_{3.41}$ ,  $\text{SrNbO}_{3.45}$ , and  $\text{SrNbO}_{3.50}$  for Eka;b. A contribution of itinerant electrons appears in the Eka spectra: A Drude peak is observed for  $\text{SrNbO}_{3.45}$ , which is even more pronounced for  $\text{SrNbO}_{3.41}$  in full agreement with the higher density of conduction electrons for the latter compound, while the absence of a Drude peak for  $\text{SrNbO}_{3.50}$  accounts for its insulating character.

Despite their layered crystal structure,  $\text{SrNbO}_{3.45}$  and  $\text{SrNbO}_{3.41}$  show a pronounced quasi-1D metallic character which can be related to the chain-like arrangement of  $\text{NbO}_6$  octahedra along the a axis. A more detailed picture is provided by band structure calculations in the lo-

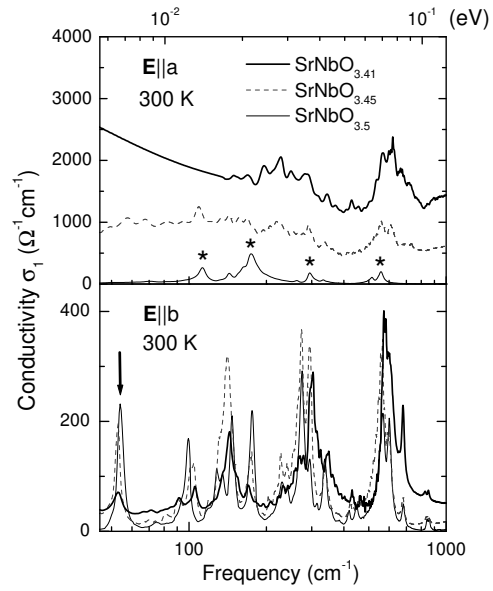


FIG. 10. Optical conductivity  $\sigma_1$  of  $\text{SrNbO}_{3.50}$ ,  $\text{SrNbO}_{3.45}$ , and  $\text{SrNbO}_{3.41}$  at RT for Eka and Ekb, respectively. The asterisks mark the phonon lines of  $\text{SrNbO}_{3.50}$  for Eka which survive in the conducting compounds. The arrow indicates the ferroelectric soft mode of  $\text{SrNbO}_{3.50}$ .

cal density approximation (LDA) for  $\text{SrNbO}_{3.41}$ .<sup>1,20</sup> The predominant contribution to the DOS near  $E_F$  is attributed to the Nb site in the middle of the slab, while the other two<sup>21</sup> Nb sites contribute considerably less (see Fig. 6 (a) in Ref. 20). The corresponding  $\text{NbO}_6$  octahedra in the middle of the slabs (marked by thick lines in Fig. 1) are the least distorted ones, with the Nb atoms located right in the center of the octahedra; for all other octahedra the Nb atoms are considerably shifted away from the central octahedral position. The quasi-1D metallic character is thus related to the central chains of least distorted octahedra in the middle of the slabs. The influence of the central octahedral chains on the electronic characteristics is illustrated by the experimental results of  $\text{Sr}_{0.8}\text{La}_{0.2}\text{NbO}_{3.50}$  compared to those of  $\text{SrNbO}_{3.41}$ : Both compounds nominally contain the same density of Nb4d conduction electrons (see Table I). However, in  $\text{Sr}_{0.8}\text{La}_{0.2}\text{NbO}_{3.50}$  the slabs are only four octahedra wide, i.e., the central chains are missing. According to the resistivity<sup>3</sup> and optical results presented here, this compound shows a much weaker metallic behavior compared to  $\text{SrNbO}_{3.41}$ , and the quasi-1D character of its band structure, as observed by ARPES, has almost vanished. This is in agreement with the absence of a gap opening for  $\text{Sr}_{0.8}\text{La}_{0.2}\text{NbO}_{3.50}$  along the chains (see Fig. 11): The intensity of the weak Drude peak observed in the RT optical conductivity for Eka has decreased at 5 K, but a low-frequency peak has not developed, in contrast to what is found for  $\text{SrNbO}_{3.41}$  and  $\text{SrNbO}_{3.45}$ . All these experimental findings show that the quasi-1D metallic character and the related gap opening observed for  $\text{SrNbO}_{3.41}$  and  $\text{SrNbO}_{3.45}$  are indeed linked to the central octahedral

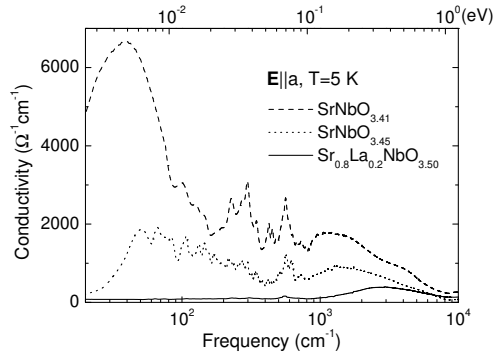


FIG. 11. Optical conductivity  $\sigma_1$  of  $\text{SrNbO}_{3.41}$ ,  $\text{SrNbO}_{3.45}$ , and  $\text{Sr}_{0.8}\text{La}_{0.2}\text{NbO}_{3.50}$  at 5 K for E||a.

chains.

The compounds  $\text{SrNbO}_{3.50}$ ,  $\text{SrNbO}_{3.45}$ , and  $\text{SrNbO}_{3.41}$  have a complex crystal structure and thus exhibit rich phonon spectra for both polarization directions (see Fig. 10). For E||a the main groups of phonon modes observed for  $\text{SrNbO}_{3.50}$ , which are centered around 110, 170, 300, and 540  $\text{cm}^{-1}$  and marked by asterisks in Fig. 10, survive in the conducting members, with only small frequency shifts and a masking due to the contribution of itinerant electrons. The similarities in the vibrational properties are more obvious for the polarization direction perpendicular to the chains, E||b, since no D rude contribution is present: The main groups of phonon lines, centered around 53, 100, 150, 290, and 600  $\text{cm}^{-1}$ , are present in all three compounds. A qualitative assignment to the lattice dynamics can be achieved by a comparison with other niobium oxides with a similar network of corner-sharing  $\text{NbO}_6$  octahedra: The high-frequency infrared-active modes of  $\text{KNbO}_3$  ( $\text{NaNbO}_3$ ) were assigned to the internal modes of  $\text{NbO}_6$  octahedra, namely the 660 (675) and 550 (510)  $\text{cm}^{-1}$  modes to the stretching modes and the 375 (375)  $\text{cm}^{-1}$  mode to the bending mode.<sup>22</sup> This is in agreement with later Raman and infrared measurements on  $\text{LiNbO}_3$  and  $\text{Ba}_2\text{NaNb}_5\text{O}_{15}$ .<sup>23</sup> The lower-frequency lines ( $< 200 \text{ cm}^{-1}$ ) were assigned to translational modes of the cations.<sup>23</sup> The influence of La doping on the optical properties is illustrated in Fig. 12 where we plot the conductivity spectra of  $\text{SrNbO}_{3.50}$  and  $\text{Sr}_{0.8}\text{La}_{0.2}\text{NbO}_{3.50}$ . For E||a an electronic background related to itinerant carriers in the  $\text{Sr}_{0.8}\text{La}_{0.2}\text{NbO}_{3.50}$  spectrum is visible. Two of the main groups of phonon modes of  $\text{SrNbO}_{3.50}$  (marked by asterisks) are also present in the (weakly) conducting material, but they are broader and strongly damped. Interestingly, the relatively strong modes observed in  $\text{SrNbO}_{3.50}$  around 110 and 170  $\text{cm}^{-1}$  appear to be completely suppressed in  $\text{Sr}_{0.8}\text{La}_{0.2}\text{NbO}_{3.50}$ , indicating a strong damping of the cation translational modes by partial substitution of Sr by La. Along the b direction the similarities in the vibrational properties are also obvious. In particular, the mode around 54  $\text{cm}^{-1}$  for E||b, indicated by an arrow in Fig. 10 and 12 is present in all four compounds discussed here. For  $\text{SrNbO}_{3.50}$  this

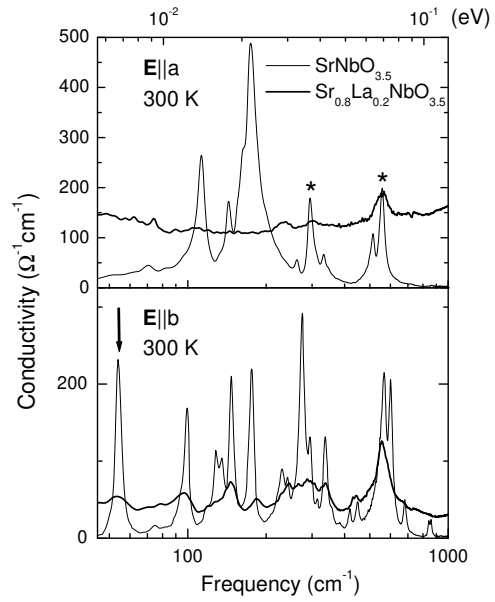


FIG. 12. Optical conductivity  $\sigma_1$  of  $\text{SrNbO}_{3.50}$  and  $\text{Sr}_{0.8}\text{La}_{0.2}\text{NbO}_{3.50}$  at RT for E||a and E||b, respectively. The asterisks mark the phonon lines of  $\text{SrNbO}_{3.50}$  for E||a which survive in the conducting compound. The arrow indicates the ferroelectric soft mode of  $\text{SrNbO}_{3.50}$ .

mode was assigned to the soft mode of the ferroelectric phase transition at 1615 K, based on Raman scattering experiments.<sup>16</sup> It was also observed in recent optical measurements and related to  $\text{NbO}_6$  octahedra tiltings.<sup>17</sup> In agreement with Ref. 17, this soft mode is temperature independent between 300 and 100 K and shifts to higher frequencies below 100 K. The precise temperature dependence is, however, difficult to determine due to the overlap with another mode which appears around 50  $\text{cm}^{-1}$  at 100 K during cooling down.

Finally, we want to discuss the puzzling electronic properties of the conducting members of the present niobate series at low temperature, in particular the opening of an energy gap at  $E_F$  found for  $\text{SrNbO}_{3.41}$  and  $\text{SrNbO}_{3.45}$ . Several aspects make an explanation of the gap opening in terms of a Peierls-type scenario most likely: (i) The FS nesting<sup>1</sup> could drive the lattice towards a Peierls distortion; (ii) the shadow band observed for  $\text{SrNbO}_{3.41}$  in ARPES<sup>2</sup> would be consistent with a superstructure with wave vector  $q = 2k_F$ ;<sup>24</sup> (iii) the appearance of phonon lines with decreasing temperature suggests a structural phase transition such as a Peierls instability. However, there remain some inconsistencies within a Peierls scenario: In contrast to what is expected for CDW formation, no sharp anomaly is found in dc resistivity; neither do thermal expansion measurements<sup>25</sup> show indications of a structural phase transition. Furthermore, an estimate of the mean-field transition temperature based on the observed gap size is not compatible with the temperature development of dc resistivity and optical conductivity.<sup>2</sup>



Further open issues are the transport mechanism in  $\text{SrNbO}_{3.41}$  and  $\text{SrNbO}_{3.45}$  along the chain direction and the closely related temperature dependence of the dc resistivity  $\rho_a$ , showing different regimes. The strong upturn of  $\rho_a$  below 50 K with cooling down can be explained by the opening of a gap, in agreement with ARPES and optics. The temperature dependence above 50 K may be due to contributions of quasiparticles with different characteristics. While the metallic temperature dependence between 50 K and 130 K suggests a band-like motion of electrons, above 130 K the hopping of more localized charge carriers appears to dominate. A possible mechanism for the localization/trapping of charge carriers could be strong electron-phonon coupling, which might also explain the observation of a pronounced MIR absorption band in the optical conductivity along the chain direction (see Figs. 4 and 7). Similar absorption bands in related quasi-1D metallic compounds were recently interpreted in terms of excitations of polaronic quasiparticles.<sup>26;27</sup> Further spectroscopic information, e.g., from temperature-dependent ARPES measurements, is needed to clarify a possible polaron formation in the studied niobates.

In conclusion, we determined the electronic and vibrational properties of the perovskite-related compounds  $\text{Sr}_{1-y}\text{La}_y\text{NbO}_{3.5-x}$  and related the results to their crystal structure. A possible transport mechanism of  $\text{SrNbO}_{3.41}$  and  $\text{SrNbO}_{3.45}$  was discussed and the importance of electron-phonon coupling in these systems suggested, possibly leading to polaron formation. To explain the low-temperature behavior a Peierls picture appears to be the most appropriate, but is insufficient to describe all the findings. An important aspect might be the close structural analogy of the quasi-1D metals  $\text{SrNbO}_{3.41}$  and  $\text{SrNbO}_{3.45}$  to the ferroelectric  $\text{SrNbO}_{3.50}$ :  $\text{SrNbO}_{3.41}$  (and the ( $n=5$ )-slabs in  $\text{SrNbO}_{3.45}$ ) contains the same structural building blocks as  $\text{SrNbO}_{3.50}$ , but with additional chains of basically undistorted  $\text{NbO}_6$  octahedra inserted in the center of the slabs. Ferroelectric  $\text{SrNbO}_{3.50}$  shows relatively high values of the static dielectric constant  $\epsilon_1$  at RT ( $\epsilon_{1a}=75$ ,  $\epsilon_{1b}=43$ , and  $\epsilon_{1c}=46$ )<sup>8</sup> indicating highly polarizable structural units. A further important result is the observation of the phonon mode at  $54\text{ cm}^{-1}$  in the E<sub>kb</sub> conductivity spectra of all present niobate compounds (see Fig. 10 and 12), which for  $\text{SrNbO}_{3.50}$  can be assigned to the ferroelectric soft mode. Since the soft modes in ferroelectrics in general lead to electrical polarization, the presence of the  $54\text{ cm}^{-1}$  mode in  $\text{SrNbO}_{3.41}$  and  $\text{SrNbO}_{3.45}$  indicates a polarizability of their lattices. The highly conducting channels of octahedra in the middle of the slabs, which are responsible for the 1D metallic transport, can thus be viewed as embedded in a highly polarizable medium, and a certain influence of this medium on the electronic properties of the chains is conceivable. This picture is, however, speculative since to our knowledge a 1D model taking into account such a polarizable medium surrounding the conducting entities does not exist.

By angle-resolved photoemission spectroscopy and polarization-dependent reflectivity measurements in the infrared we studied the electronic and vibrational properties of several members of the series  $\text{Sr}_{1-y}\text{La}_y\text{NbO}_{3.50-x}$  ( $0 \leq x \leq 0.1$ ) along and perpendicular to the chains of  $\text{NbO}_6$  octahedra.  $\text{SrNbO}_{3.50}$  is a ferroelectric insulator with a rich phonon spectrum for both polarization directions E<sub>ka</sub>;b. At room temperature the compounds  $\text{SrNbO}_{3.41}$  and  $\text{SrNbO}_{3.45}$  exhibit a metallic behavior with a strongly dispersing band along the chains (E<sub>ka</sub>) and an insulating, nondispersive character in the perpendicular direction (E<sub>kb</sub>); they are thus quasi-1D metals. Despite the similar carrier density, for  $\text{Sr}_{0.8}\text{La}_{0.2}\text{NbO}_{3.50}$  the quasi-1D metallic character is much less developed. Based on a comparison between the experimental results of  $\text{SrNbO}_{3.41}$ ,  $\text{SrNbO}_{3.45}$ , and  $\text{Sr}_{0.8}\text{La}_{0.2}\text{NbO}_{3.50}$  the quasi-1D metallic character observed in this series can be related to the central chains of least distorted octahedra located in the middle of the slabs. This is in full agreement with the results from LDA band structure calculations. We propose a possible transport mechanism for the compounds  $\text{SrNbO}_{3.41}$  and  $\text{SrNbO}_{3.45}$ , with a band-like contribution of mobile carriers and a contribution due to the hopping motion of more localized charges dominating above 130 K. At low temperature the opening of an extremely small energy gap at  $E_F$  is observed for  $\text{SrNbO}_{3.41}$  and  $\text{SrNbO}_{3.45}$  along the chain direction, which might be related to a Peierls-type instability, with electron-phonon coupling as the driving mechanism. However, not all findings can be explained within a Peierls picture, and we speculate that the highly polarizable structural units surrounding the conducting channels might have an appreciable influence.

#### Acknowledgements

We are grateful to L. Perfetti, C. Rojas, and I. Vobornik for valuable technical help. We thank H. W. Inter for fruitful discussions. Financial support by the DAAD, the BMBF (project No. 13N 6918/1), and the Deutsche Forschungsgemeinschaft is gratefully acknowledged.

---

Present address: General Physics Institute, Russian Academy of Sciences, Vavilov 38, Moscow 117942, Russia.

<sup>1</sup> C. A. Kuntscher, S. Gerhold, N. Nucker, T. R. Cummins, D.-H. Lu, S. Schuppler, C. S. Gopinath, F. Lichtenberg, J. Mannhart, K.-P. Bohnen, Phys. Rev. B 61, 1876 (2000).

<sup>2</sup> C. A. Kuntscher, S. Schuppler, P. Haas, B. Gorshunov, M. Dressel, M. Groni, F. Lichtenberg, A. Herberger,

- F. Mayer, and J. Mannhart, Phys. Rev. Lett. 89, 236403 (2002).
- <sup>3</sup> F. Lichtenberg, A. Hermberger, K. Wiedenmann, and J. Mannhart, Prog. Solid State Chem. 29, 1 (2001).
- <sup>4</sup> S. C. Abraham, H. W. Schmalz, T. Williams, A. Reller, F. Lichtenberg, D. Widmer, J. G. Bednorz, R. Spreiter, Ch. Bosshard, and P. Gunter, Acta Cryst. B 54, 399 (1998).
- <sup>5</sup> T. Williams, F. Lichtenberg, D. Widmer, J. G. Bednorz, and A. Reller, J. Solid State Chem. 103, 375 (1993).
- <sup>6</sup> J. G. Bednorz, K. H. Wächter, R. Broom, and D. Ariosa, in High- $T_c$  superconductivity 1996: Ten Years after the discovery, edited by E. Kalkis, E. Liarokapis, and K. A. Müller (Kluwer, Dordrecht, 1997).
- <sup>7</sup> S. Nanamatsu, M. Kikura, K. Doi and M. Takahashi, J. Phys. Soc. Jpn. 30, 300 (1971);
- <sup>8</sup> S. Nanamatsu, M. Kikura, and T. Kawamura, J. Phys. Soc. Jpn. 38, 817 (1975).
- <sup>9</sup> K. Ohi, M. Kikura, H. Ishida, and H. Kakinuma, J. Phys. Soc. Jpn. 46, 1387 (1979).
- <sup>10</sup> J.-E. Weber, C. Kögler, N. Buttgen, H.-A. Kug von Nidda, A. Loidl, and F. Lichtenberg, Phys. Rev. B 64, 235414 (2001).
- <sup>11</sup> V. Bobnar, P. Lunkenheimer, J. Hemberger, A. Loidl, F. Lichtenberg, and J. Mannhart, Phys. Rev. B 65, 155115 (2002).
- <sup>12</sup> G. V. Kozlov and A. A. Volkov, in Millimeter and Submillimeter Wave Spectroscopy of Solids, ed. G. Gruner (Springer, Berlin, 1998).
- <sup>13</sup> M. Dressel and G. Gruner, Electrodynamics in solids: Optical properties of electrons in matter (Cambridge University Press, Cambridge, 2002).
- <sup>14</sup> C. A. Kuntscher, PhD thesis, Universität Karlsruhe (Cuvillier Verlag, Göttingen, 2000).
- <sup>15</sup> L. Pintschovius, unpublished.
- <sup>16</sup> K. Ohi and S. Kojima, Japan. J. Appl. Phys. 24, 817 (1985).
- <sup>17</sup> E. Buxaderas, S. Kamba, and J. Petzelt, J. Phys.: Condens. Matter 13, 2823 (2001).
- <sup>18</sup> D. H. Lu, C. S. Gopinath, M. Schmidt, T. R. Cummins, N. Nucker, S. Schuppler, and F. Lichtenberg, Physica C 282-287, 995 (1997).
- <sup>19</sup> No dc resistivity data are available for  $\text{SrNbO}_{3.45}$ , but it is expected to be qualitatively similar to those of  $\text{Sr}_{0.96}\text{Ba}_{0.04}\text{NbO}_{3.45}$  which has the same crystal structure<sup>3</sup> and, within an ionic picture, the same electron doping as  $\text{SrNbO}_{3.45}$ .
- <sup>20</sup> H. Winter, S. Schuppler, and C. A. Kuntscher, J. Phys. Cond. Matter 12, 1735 (2000).
- <sup>21</sup> There are three inequivalent Nb sites per unit cell in  $\text{SrNbO}_{3.41}$ , as was illustrated in Ref. 20.
- <sup>22</sup> J. T. Last, Phys. Rev. 105, 1740 (1957);
- <sup>23</sup> S. D. Ross, J. Phys. C 3, 1785 (1970).
- <sup>24</sup> J. Voit, L. Perfetti, F. Zwick, H. Berger, G. Margaritondo, G. Gruner, H. Höchst, and M. G. Rioni, Science 290, 501 (2000).
- <sup>25</sup> P. Nagel, V. Pasler, and C. Meingast, unpublished.
- <sup>26</sup> C. Presura, M. Popinciuc, P. H. M. van Loosdrecht, D. van der Marel, M. Mostovoy, T. Yamachi, and Y. Ueda, Phys. Rev. Lett. 90, 026402 (2003).
- <sup>27</sup> C. A. Kuntscher, D. van der Marel, M. Dressel, F. Lichtenberg, and J. Mannhart, Phys. Rev. B 67, 035105 (2003).